# Our Magphan RT family continues to grow to meet QA needs for MR imaging of large fields of view.


The modular design enables the Magphan® RT phantom to be handled by a single person without special equipment. The three-piece configuration measures geometric distortion and uniformity along with tests for laser alignment, slice thickness, resolution, and Signal-to-Noise Ratio. The central section contains 24 contrast spheres that cover a range of T1, T2, and ADC values, as well as two slice thickness ramps.

**The Phantom Laboratory manufactures high-precision phantoms coupled with Smári image analysis service and innovative custom solutions for the medical imaging and radiation therapy fields.**

---

**Click to view our phantoms and schedule a demo of our Smári image analysis service.**

phantomlab

phantomlab.com

Received: 17 August 2021 | Revised: 17 August 2021 | Accepted: 26 September 2021

DOI: 10.1002/mp.15292

RESEARCH ARTICLE

MEDICAL PHYSICS

# Compensating for beam modulation due to microscopic lung heterogeneities in carbon ion therapy treatment planning

**Athena Evalour Simbahon Paz**[1] | **Kilian-Simon Baumann**[2,3] | **Uli Andreas Weber**[1] | **Matthias Witt**[2] | **Klemens Zink**[2,3] | **Marco Durante**[1,4] | **Christian Graeff**[1,5]

[1] GSI Helmholtzzentrum für Schwerionenforschung GmbH, Darmstadt, Germany

[2] Marburg Ion-Beam Therapy Center (MIT), Marburg, Germany

[3] Institute of Medical Physics and Radiation Protection, University of Applied Sciences, Giessen, Germany

[4] Institute for Condensed Matter Physics (CG), Technical University, Darmstadt, Germany

[5] Department of Electrical Engineering and Information Technology, Technical University, Darmstadt, Germany

**Correspondence**
Christian Graeff, Planckstraße 1, 64291 Darmstadt, Germany.
Email: c.graeff@gsi.de

## Abstract

**Purpose**: To predict and mitigate for the degradation in physical and biologically effective dose distributions of particle beams caused by microscopic heterogeneities in lung tissue.

**Materials and Methods**: The TRiP98 treatment planning system was adapted to account for the beam-modulating effect of heterogeneous lung tissue in physical and biological inverse treatment planning. The implementation employs an analytical model that derives the degradation from the established "modulation power" parameter $P_{\mathrm{mod}}$ and the total water-equivalent thickness of lung parenchyma traversed by the beam. Beam modulation was reproduced through an on-the-fly convolution of the reference Bragg curve with Gaussian kernels depending on the modulation power of lung tissue (upstream). For biological doses, the degradation was determined by modulating dose-averaged $\alpha$, $\beta$, and LET distributions. Carbon SOBP measurements behind lung substitute material were performed to validate the code. The implementation was then applied to a phantom and patient case.

**Results**: Experimental results show the passage through a 20-cm Gammex LN300 slab led to a decrease in target coverage and broadening of the SOBP distal fall-off. However, dose coverage was regained through optimization. A good agreement between calculated and measured SOBPs was also found. In addition, a patient case study revealed a 3.2% decrease in $D_{95}$ from degradation ($P_{\mathrm{mod}} = 450\ \mu$m), which was reduced to a 0.4% difference after optimization. Furthermore, widening of the RBE distribution beyond the target distal edge was observed. This implies an increased degradation in the biological dose, which could be harmful to healthy tissues distal to the target.

**Conclusions**: This is the first implementation capable of compensating for lung dose perturbations, which is more effective than margin extensions. A larger patient study is needed to examine the observed modulation in the RBE distribution and judge the clinical relevance also in IMPT, where margins might prove insufficient to recover target coverage.

# 1 | INTRODUCTION

Tissue inhomogeneity has long been considered as a source of uncertainty for particle therapy.[1] Early studies have shown that density heterogeneities in the beam path cause changes to the energy spectrum, which then leads to the degradation of the Bragg peak and broadening of the distal fall-off.[1–3] This is of particular concern for the treatment of lung tumors where microscopic, lung soft tissue-to-air interfaces exist. However, these porous microstructures are not captured by conventional CT scanners due to limitations in resolution.[4–6] Consequently, heterogeneities in lung tissue are not accounted for during treatment planning and the resulting Bragg peak degradation cannot be considered accurately during the dose calculation. This can lead to inadequate dose to the target volume and unwanted dose to normal tissues.[7]

In order to address the potential dose uncertainties, several works have focused on establishing an analytical model for the Bragg peak degradation. It was found that the distribution of traversed water-equivalent thickness in the porous material can be approximated by a Gaussian function.[8] The modulated depth-dose curve can then be estimated from the convolution of the pristine Bragg curve and the derived Gaussian function.[5] In addition, the degradation was reproduced by modulating the density of individual voxels in the CT image based on a density distribution obtained from the Gaussian function.[9] Following this technique, Monte Carlo-based treatment planning studies were performed both on phantom and patient cases. An increase in the degradation was observed with decreasing tumor volume and increasing depth within the lung.[6,9,10] However, also a deterministic treatment planning program like TRiP98 can be used to assess the degradation from lung modulation by overlaying a series of dose distributions (typically $n = 50–100$) with resampled density distributions.[11] An inherent disadvantage of these approaches, however, is that multiple recalculations of the plan are required to sufficiently sample the density distribution. This permits forward dose calculation at very long calculation times, which is incompatible with clinical treatment planning processes. Moreover, a consideration in inverse treatment plan optimization is not possible. Recently, the degradation model was implemented into the dose calculation algorithm of the matRad treatment planning toolkit and used to evaluate the beam-modulation effect on a patient cohort treated with proton therapy.[12] Their results showed that for a deep-seated, small tumor volume, the target underdosage increased by up to 26%. These works have so far investigated the modulation effects only on the physical dose calculation. Nevertheless, in order to mitigate for this effect, the Bragg peak degradation has to be accounted for also in the dose optimization stage.

In this study, we demonstrate the mitigation of dose perturbations due to microscopic lung heterogeneities using the TRiP98 treatment planning system with some additionally implemented analytical formula in order to avoid time consuming random procedures. The degradation model was implemented not only in the calculation of physical dose but also extended to the absorbed dose optimization. The implementation is also capable of predicting and compensating for degradations in biologically effective doses for treatments with carbon ions. This study is the first to include beam-modulating effects in the physical and biological inverse treatment planning, which is suitable in a clinical setting.

# 2 | MATERIALS AND METHODS

## 2.1 | Mathematical model for Bragg peak degradation

Monoenergetic charged particles traveling through a porous material follow different paths in a locally changing density distribution. As a result, the particles experience a fluctuation in energy loss in addition to the energy-loss straggling incurred from the large number of collisions in the slowing-down process.[13,14] The increased energy spread of the particles then leads to a broadening of the Bragg peak. To model this phenomenon, the porous material can be represented by a binary voxelized geometry.[5,9,15] In the case of the human lung, the highly heterogeneous, microscopic structure of lung parenchyma is replicated by dividing the lung model into sub-millimeter sized cubic voxels, which are randomly filled with either lung tissue or with air.[9] Each path across the voxelized lung traverses a different sequence of lung tissue and air voxels and, therefore, impart a different water-equivalent thickness. The probability that a beam path has a water-equivalent thickness $t'$ can be approximated by a Gaussian distribution,

$$P(t'|\sigma(z), t_L(z)) = \frac{1}{\sqrt{2\pi}\sigma(z)} \exp\left(\frac{-(t' - t_L(z))^2}{2(\sigma(z))^2}\right), \quad (1)$$

where $t_L(z) = \sum_i t_i$ is the total water-equivalent path length of lung voxels $t_i$ upstream of the water-equivalent depth $z$, and

$$\sigma(z) = \sqrt{P_{\text{mod}} \cdot t_L(z)}. \quad (2)$$

The modulation power $P_{\text{mod}}$ is a characteristic measure of the degree of degradation.[8,15] This material-specific quantity varies according to the size of the microscopic fine structure making up the porous material. The larger the structure size, the stronger is the

induced degradation. Typical modulation power values determined from porcine lungs have been reported to be in the range of 250–450 $\mu$m.[8,10,12] The variation in the measured values is attributed to the spatial deviation in structure size throughout the lung. A higher modulation effect is expected in the central lung regions where the structure size is larger than in peripheral areas.[10]

The beam modulation at the water-equivalent depth $z$ is then reproduced by convolving the pristine Bragg curve $D(z)$ with the corresponding Gaussian kernel,

$$D_{\mathrm{mod}}(z) = \int_{-\infty}^{\infty} P(t'|\sigma(z), t_L(z))\, D(z+t')dt'. \quad (3)$$

Note that the convolution is only applied for $\sigma(z) > 0$.

## 2.2 | Model implementation

In this work, the dose calculation and optimization engines of the GSI in-house treatment planning system TRiP98[16] were modified to account for beam modulation due to microscopic-scale heterogeneities in lung tissue.

### 2.2.1 | Extraction of the degree of modulation

Regions in the CT image consisting of lung parenchyma were filtered by identifying voxels with Hounsfield units (HU) in the range of −900 to −500. These HU values are consistent with the density range of 0.1–0.5 g/cm$^3$ obtained in inflated porcine lung experiments.[8,11,15] A Hounsfield-range look-up table was then used in a Siddon-based raytracing algorithm to compute the total water-equivalent path length in lung traversed by the beam for each voxel. Subsequently, the $\sigma$ values of Equation (2) were determined by assuming a constant modulation power in all voxels identified as lung parenchyma.

### 2.2.2 | Dose calculation

For physical dose, the broadened depth-dose curve was calculated by on-the-fly convolutions (Equations 1–3), applying for each depth $z$ the corresponding Gaussian kernel. For biological doses, the relative biological effectiveness (RBE) of the complex radiation field produced by a carbon ion irradiation was calculated based on the local-effect model (LEM).[16] The low-dose approximation of LEM version IV was used to generate tissue-specific input tables containing initial RBE values as a function of particle species and LET.[17,18] The dose-averaged intrinsic radio-sensitivity parameters $\alpha$ and $\beta$ for the mixed radiation field on each voxel were then computed based on these input tables. In order to determine the beam-modulating effect on biological doses, the spreading of the entire particle spectra in depth has to be replicated. Modulating the full spectra, however, entails the convolution of individual particle distributions for all energy bins and for all primary and secondary particles. Performing such a computation per voxel would significantly slow down the dose calculation. Therefore, a more efficient approach is adopted by performing the convolution directly with the dose-averaged $\alpha$, $\beta$, and LET distributions of the unperturbed beam with the same concept as the convolution of the depth dose distribution (see Equation 3). The calculation speed was further improved by applying a Fast Fourier transform (FFT) to carry out the convolution. As the computation solely involved real-valued functions, symmetries of the Fourier transform were exploited, which enabled the evaluation of two functions in a single FFT operation.[19]

## 2.3 | Experimental validation

In order to validate the implementation of the degradation model, measurements were performed at the Marburg Ion-Beam Therapy Center (MIT), Marburg, Germany. A diagram of the experimental setup is shown in Figure 1. A 20-cm thick Gammex LN300 lung substitute material was irradiated with a pristine Bragg peak from a carbon ion beam. The modulated depth-dose distribution was acquired downstream of the sample using a water column. The laterally integrated depth dose curves for each of the nine iso-energy slices comprising the SOBP were then measured consecutively. For the Reference SOBP measurement, a 4.8-cm thick PMMA bolus was inserted in front of the water column instead of the lung substitute material. The PMMA bolus was set to have the same water-equivalent thickness as the LN300 plates to facilitate measurement at the same depth points for all the SOBPs.

Prior to the experiment, the LN300 slabs were characterized to have an effective modulation power of $P_{\mathrm{mod}} = 208\ \mu$m and a total water-equivalent thickness of $t_L = 5.76$ cm$H_2O$ through Bragg curve measurements as described in Ringbæk *et al*.[15] Two treatment plans (Reference and Optimized plans) for spread-out Bragg peaks with field sizes of $1.0 \times 1.0$ cm$^2$ and widths of 2.0 cm were generated using carbon ion energies between 257.60 MeV/u and 283.19 MeV/u. The plans used a regular grid of beam spots with a 2.0-mm spacing, an iso-energy slice spacing of 3.0-mm$H_2O$ and a 3.0-mm ripple filter. For the Optimized plan, the CT phantom consisted of a 20-cm thick lung substitute material with an HU = −716 situated in front of the 20-cm water column. The Optimized plan was then computed accounting for the beam modulation in both dose calculation and optimization stages. For the Reference plan, the lung substitute material was replaced with a 5.76-cm thick water bolus. Both plans were calculated with a

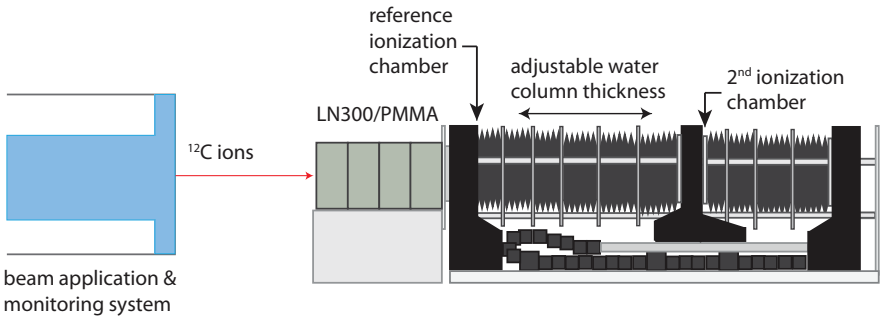


**FIGURE 1** Experimental setup. A 20-cm thick Gammex LN300 lung substitute material was irradiated with carbon ions. The modulated dose distribution was measured using a water column (PTW PeakFinder) downstream of the sample. For the reference case, the sample was replaced with a 4.8-cm thick PMMA bolus so that the same depth points can be adopted for all measurements

lateral size of $10.0 \times 10.0$ cm$^2$ to account for the 8-cm diameter active area of the water column.

During the experiment, three sets of SOBPs were measured, namely the Reference, Degraded, and Optimized SOBPs. The Reference SOBP was obtained by irradiating the 4.8-cm block of PMMA using the Reference plan. For the Degraded SOBP, the Reference plan was utilized to irradiate the LN300 slabs placed in front of the water column. Finally, the Optimized SOBP was measured downstream of the LN300 slabs using the Optimized plan.

To test the implementation against the beam-modulating effect of the lung substitute material, measured depth-dose distributions were compared with the corresponding distributions calculated in TRiP98 adopting a modulation power of $P_{\text{mod}} = 208$ $\mu$m for the LN300 plates. The agreement between measured and calculated curves were judged from their dose difference normalized to the entrance dose, that is, dose at the minimum depth point measured of 2.3 cm. For the calculated SOBPs, the impact of the degradation was evaluated according to $D_{95}$ and $V_{95}$ values at the target region. The distal fall-off widths were also determined from the distance required for the dose distribution to fall from 80% to 20% of the prescribed dose distal to the uniform dose region of the SOBP.[5]

## 2.4 | Verification of the spectral convolution

A sample spectral base data from TRiP98 for a 270.55-MeV/u carbon ion was used to ascertain the broadening of the entire particle spectra in depth caused by the traversal through the 20-cm LN300 plates. The spectral data contain the energy distributions of the primary ion and secondary fragment particles per depth. To carry out the convolution of the full particle spectra, a Gaussian function was generated using a $P_{\text{mod}} = 208$ $\mu$m and water-equivalent thickness of $t_L = 5.76$ cm$H_2O$. Then for every particle species, each energy bin as a function of depth was convolved with the Gaussian kernel through a Matlab script. The depth dose distribution was obtained from the convolved spectra along with an energy loss table as in Krämer *et al*.[20] The biological dose was also determined following the approach outlined in Krämer and Scholz.[16] The RBE distribution was computed from the ratio of biological to physical dose. The corresponding physical, biological depth-dose distributions, and RBE profile were then calculated using the FFT-based TRiP98 implementation to verify that the full spectral convolution can be accurately replicated.

## 2.5 | Patient data and treatment planning

The modified biological dose calculation and optimization algorithms were tested on a sample patient case diagnosed with stage I NSCLC. The patient was originally treated with photon SBRT at the Champalimaud Centre for the Unknown in Lisbon, Portugal. The patient 4DCT was obtained with 10 motion phases. Target and OAR contours, which were delineated in the end-inhale reference phase, were propagated to other motion phases through deformable image registration (DIR). The clinical target volume (CTV) was 1.6 cm$^3$ in size and was situated in the left superior lung.[21]

The plan was recalculated for a carbon ion therapy treatment using a fraction dose of 3.5 GyE in accordance with a regimen of 70 GyE in 20 fractions prescribed for centrally located disease at Shanghai Proton and Heavy Ion Center (SPHIC).[22] The biologically effective doses were computed using LEM IV assuming an $\alpha/\beta$ of 6 and 2 for the target and for OARs, respectively. To model the beam-modulation effect, two different modulation power values were investigated, namely $P_{\text{mod}} = 256$ $\mu$m and 450 $\mu$m. This covers the range of modulation power values recently reported in literature.[10,12] For the treatment planning, the CTV was expanded with a 3-mm isotropic margin to account for setup uncertainties. A range-considering ITV for a single oblique field was then constructed on the expanded CTV from the patient 4DCT.[23] A beam spot with a 6.0-mm FWHM in a regular grid spacing of 2.0 mm, an iso-energy slice spacing of

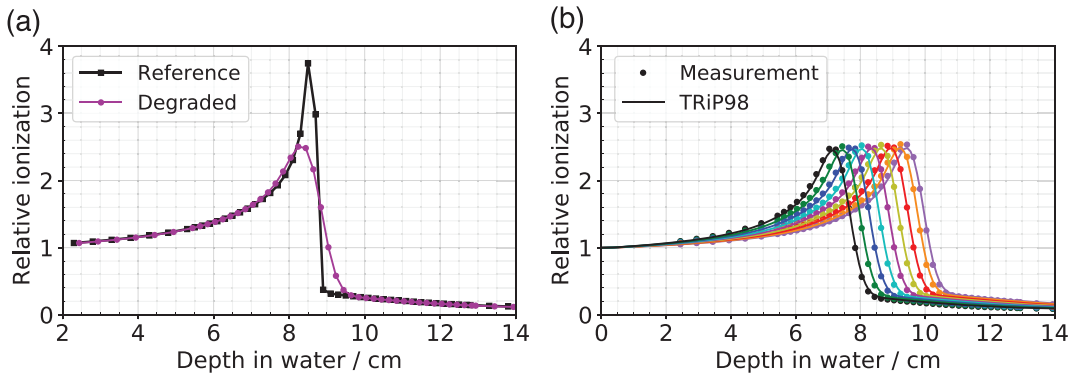


**FIGURE 2** (a) Laterally integrated depth dose curves measured from a 271.13-MeV/u carbon ion beam passing through a 4.8-cm PMMA bolus (Reference curve) and a 20-cm Gammex LN300 lung substitute material (Degraded curve). The minimum depth point measured is at 2.3 cm. (b) Calculated Bragg curves assuming a modulation power of $P_{mod} = 208\ \mu m$ are superimposed on measured data points. The nine different colors correspond to the nine Bragg peaks that comprise the Degraded SOBP

3.0-mm$H_2O$, and a 3.0-mm ripple filter were also used in the planning. To isolate the effects of Bragg peak degradation from that of target motion, the fraction dose was assumed to be delivered equally among the 10 motion phases.[24]

The impact of the Bragg peak degradation on the dose distribution was assessed based on $D_{95}$ and $V_{95}$ values evaluated on the CTV. Furthermore, dose to normal tissues around the target volume was determined from the mean dose received by a 13-mm thick spherical shell around the CTV.

## 3 | RESULTS AND DISCUSSIONS

### 3.1 | Estimation of degradation in the physical dose calculation

Figure 2(a) shows a comparison between the reference Bragg curve and the dose distribution measured downstream of the 20-cm Gammex LN300 slab for an incident 271.13-MeV/u carbon ion beam. In the modulated scenario, carbon ions incurred additional energy loss straggling as they traverse through the lung substitute material. The added straggling, however, has a negligible effect on the absorbed dose at the entrance channel. Consequently, the reference and modulated Bragg curves coincide at the plateau region. But as the particles slow down, the influence of the increased energy loss straggling becomes prominent, resulting in the broadening of the Bragg peak. Overall, the effect leads to a reduction in the peak-to-plateau ratio and the widening of the distal fall-off. A spreading of the dose is also observed at the proximal side of the Bragg peak albeit at a lesser extent than at the distal edge.

Depth-dose distributions measured from nine carbon beam energies that constitute the Degraded SOBP are depicted in Figure 2(b). The corresponding calculated Bragg curves are plotted against the measured data points. As seen in Figure 2(b), the calculated Bragg curves fitted the measured ones accurately. The mean dose difference did not exceed 1.5%. This result demonstrates the capability of the modified dose calculation engine to accurately predict the degradation in the absorbed dose given the modulation power of the porous material traversed by the beam.

### 3.2 | Recovery of target coverage

Calculated depth-dose curves along the central beam axis of the Reference, Degraded, and Optimized SOBPs are given in Figure 3(a). The corresponding dose-volume histograms (DVH) are presented in Figure 3(b). As a consequence of the Bragg peak degradation, a 56.0% increase in the distal fall-off is observed on the Degraded SOBP relative to the Reference SOBP. An inadequate dose is given to the target volume, which is indicated by low $D_{95}$ and $V_{95}$ values of 80.7% and 78.3%, respectively. To compensate for these dose perturbations, the degradation model was then applied in the dose optimization stage. A considerable improvement in target coverage is achieved with a $V_{95}$ of 98.9%. Underdosage in the target region is also avoided yielding a $D_{95}$ of 97.8%. As depicted in Figure 3(a) and (b), a sufficient target coverage is regained as a result of the optimization. However, the extension of the distal fall-off cannot be corrected by the optimization. These findings are consistent with experimental results shown in Figure 3(c). At the target region, while a clear underdosage is found for the Degraded SOBP (green squares), the laterally integrated dose distribution of the Optimized case (red triangles) matches that of the Reference SOBP (black circles). A comparison between calculated and measured laterally integrated dose profiles also shows a good agreement with mean dose differences not exceeding 1.8%.

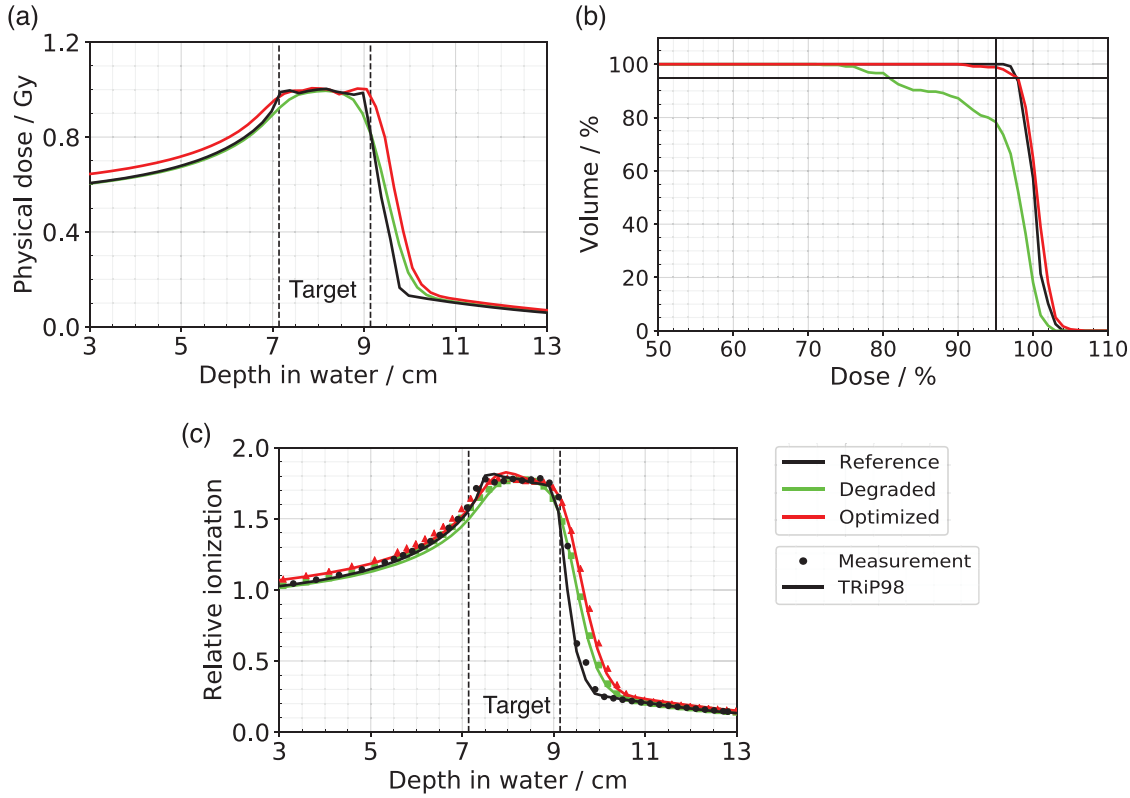


**FIGURE 3** (a) Depth-dose profiles along the central beam axis of a 2-cm SOBP calculated with TRiP98 for the Reference, Degraded, and Optimized cases. (b) Dose-volume histograms resulting from the dose distributions in (a). $D_{95}$ and $V_{95}$ are indicated by solid black horizontal and vertical lines, respectively. (c) Calculated (solid lines) and measured (symbols) laterally integrated dose distributions for the Reference, Degraded, and Optimized SOBPs

## 3.3 | The influence of the degradation to the biological dose

The impact of the degradation to the primary carbon ion spectra and exemplary secondary particle spectra from a 270.55 MeV/u carbon ion beam is illustrated in Figure 4(a)–(d). Secondary particles such as helium fragments have a broad energy distribution. Hence, they are barely influenced by the beam modulation. On the other hand, the broadening is more pronounced for the primary carbon ion spectra due to its initially sharp distribution. It is also worth noting that the smearing of the carbon ion distribution has led to the addition of particles from neighboring higher and lower energy bins to the energy spectrum in each depth. This change in energy spectrum per depth can cause an equivalent change to the radiation quality. To highlight the effect of this scenario, the physical and biological doses as well as the RBE distribution resulting from the full spectral convolution (performed in Matlab) are depicted in Figure 4(e)–(g) as green circles. Both physical and biological doses exhibit the characteristic features of the beam-modulating effect—a reduced dose to the Bragg peak and widened fall-off. Nevertheless, an even stronger degradation is seen in the biological dose as evident by the broader RBE distribution that extends beyond the distal edge. This is attributed to the presence of additional low-energy primary particles at the distal region as a consequence of the beam modulation. Moreover, the low absorbed dose also resulted in a high biological effectiveness at this region.[25]

Superimposed in Figure 4(e)–(g) as solid lines are the corresponding physical, biological and RBE distributions obtained from the FFT-based TRiP98 implementation. As depicted in the figure, the plots generated through a lengthy spectral convolution in Matlab are reproduced well by using the simpler convolution of the dose-averaged $\alpha, \beta$, and LET distributions. Based on these results, it can be inferred that the implementation can effectively simulate the beam-modulating effects also in the biological dose calculation.

## 3.4 | Mitigation of the Bragg peak degradation in a patient case

The 4D-dose distribution from the Reference and Degraded treatment plans computed with $P_{\text{mod}} = 450$ $\mu$m are given in Figure 5(a) and (b), respectively. Due to the tumor location, a long beam path through lung tissue

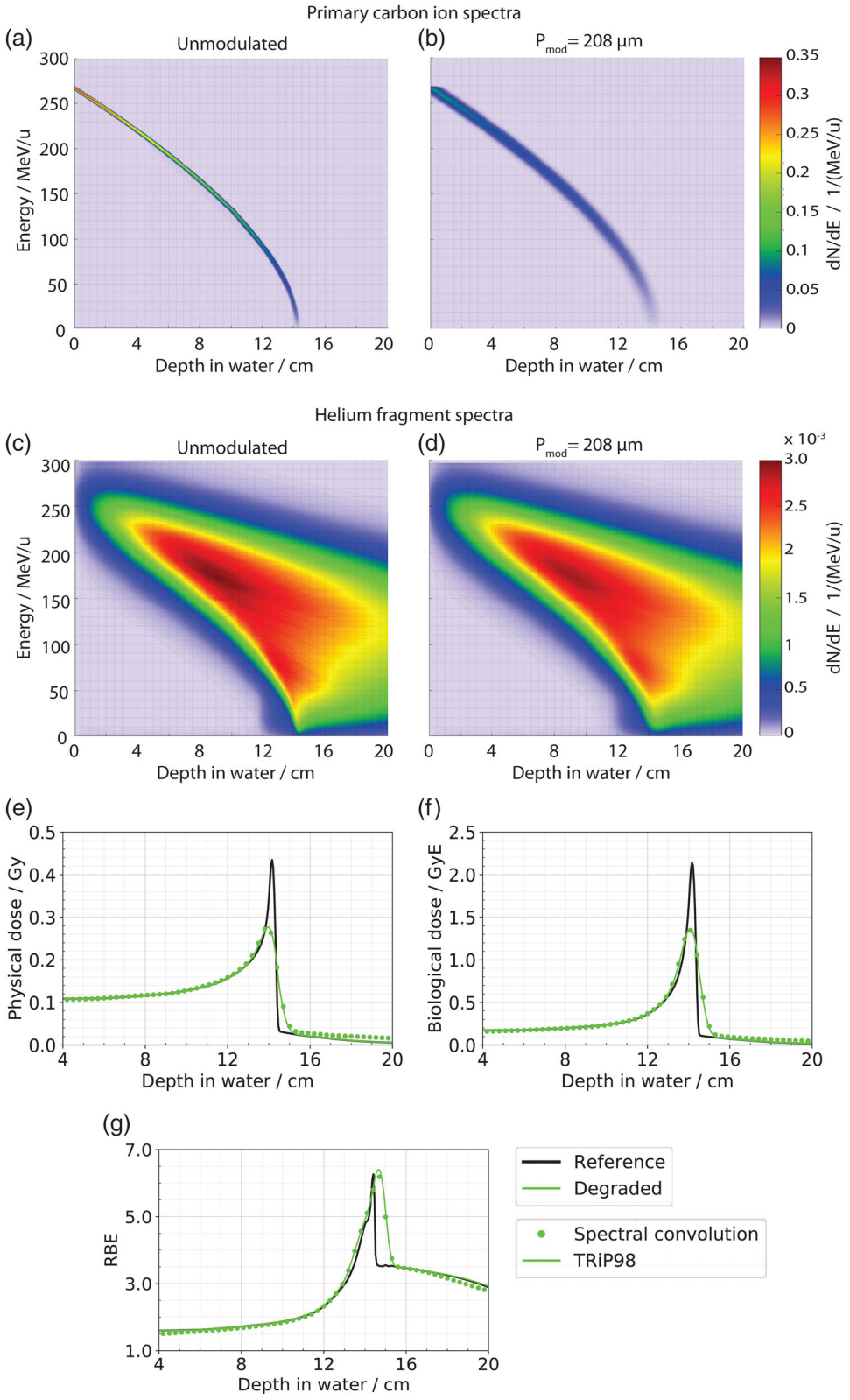


**FIGURE 4** (a and b) Spectral distribution from primary carbon ions and (c and d) helium fragments with and without modulation for an incident 270.55-MeV/u carbon ion beam. (e) The physical dose, (f) biological dose, and (g) RBE distributions resulting from the spectral modulation computed in Matlab (green circles). For comparison, the corresponding predictions from the FFT-based TRiP98 implementation are superimposed as solid lines

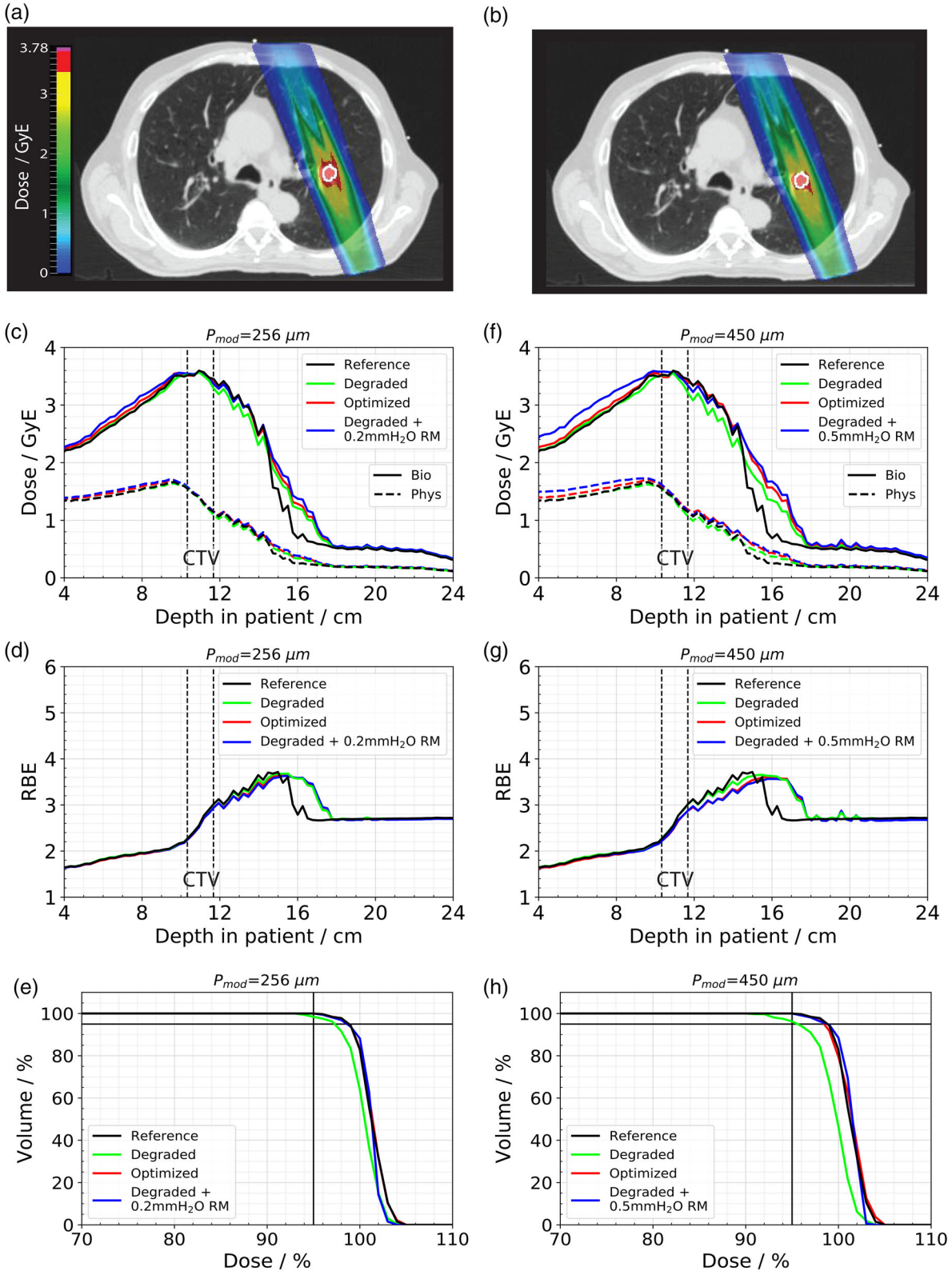


**FIGURE 5** Comparison of the 4D-dose distribution from (a) unmodulated and (b) modulated ($P_{mod}$ = 450 $\mu$m) treatment plans. The CTV contour is outlined in white. Biological and physical depth-dose profiles, RBE distributions, and DVHs from the Reference, Degraded, and Optimized plans for (c–e) $P_{mod}$ = 256 $\mu$m and (f–h) $P_{mod}$ = 450 $\mu$m. $D_{95}$ and $V_{95}$ are indicated by solid black horizontal and vertical lines on the DVH plots, respectively

**TABLE 1** Dose metrics for the patient plans shown in Figure 5. All tabulated values are percent of the planned dose (3.5 GyE) or percent of the specified volumes

| | $P_{mod}$ = 256 $\mu$m | | | $P_{mod}$ = 450 $\mu$m | | |
|---|---|---|---|---|---|---|
| | $D_{95}$ | $V_{95}$ | Shell $D_{mean}$ | $D_{95}$ | $V_{95}$ | Shell $D_{mean}$ |
| Reference | 98.8 | 100 | 62.6 | | | |
| Degraded | 97.3 | 98.4 | 61.1 | 95.6 | 96.3 | 60.1 |
| Optimized | 98.8 | 100 | 63.4 | 98.4 | 100 | 64.2 |
| Degraded + RM | 98.6 | 100 | 67.7 | 98.8 | 100 | 69.2 |

is unavoidable. As a result, the Bragg peak degradation has compromised target dose coverage as seen in Figure 5(b) as the reduction in high dose areas around the target. An expansion of the regions receiving low dose (green) can also be observed distal to the target.

Figure 5(c)–(e) shows depth-dose profiles, RBE distributions, and DVHs for the Reference, Degraded, and Optimized plans for $P_{mod}$ = 256 $\mu$m. The corresponding plots for a higher modulation power of $P_{mod}$ = 450 $\mu$m are given in Figure 5(f)–(h). The Degraded biological dose profiles exhibit underdosage particularly at the distal region of the CTV. A significant broadening of the fall-off is also observed. Although this resulted in a slightly lower dose directly behind the CTV, the dose extended further into the healthy lung tissue. The decrease in $D_{95}$ and $V_{95}$ values (see Table 1) for the Degraded plans in comparison to the Reference plan clearly point to a decrease in target coverage. For the nominal modulation power of $P_{mod}$ = 256 $\mu$m, the $D_{95}$ and $V_{95}$ were reduced by 1.5% and 1.6%, respectively, whereas for $P_{mod}$ = 450 $\mu$m, a 3.2% and 3.7% reduction were found. As the beam-modulating effect of lung tissue introduces systematic uncertainties, this level of dose perturbations will be present in all treatment fractions. Consequently, systematic deviations such as this are considered to have a larger impact than random errors, which can potentially average-out over different fractions.[26,27] Therefore, when left uncompensated, this can be detrimental to the treatment. In order to mitigate for this effect, the RBE-weighted dose was optimized accounting for the modulation in the beam path. As seen in Figure 5(c) and (e) and 5(f) and (h), a better target coverage is achieved after the optimization. The Optimized dose profiles matched the Reference profile at the target region. $D_{95}$ and $V_{95}$ values for the Reference plan were also closely matched by the Optimized plans. An alternative method to regain target coverage is to increase the proximal and distal margins on the CTV in the beam direction.[10] To test this approach against the Optimized plans, an additional range margin is employed in the ITV computation. The resulting Degraded dose profiles with the added range margins (Degraded + RM curves) are plotted in Figure 5(c) and (f). An improvement in the target coverage is also achieved as indicated by the increased $D_{95}$ and $V_{95}$ values. However, the improvement is at an expense of a much higher dose delivered to the surrounding normal tissues. For the Optimized plans, the mean dose on the shell around the CTV differs from the Reference case by 1.3% and 2.6% for $P_{mod}$ = 256 $\mu$m and 450 $\mu$m, respectively. In contrast, the added CTV margins for the corresponding modulation powers resulted in a 8.1% and 10.5% increase in dose to the healthy tissues.

Another important implication of the widened distal fall-off is the change in the RBE distribution as depicted in Figure 5(d) and (g). The Degraded plans display much broader RBE profiles than the Reference plan, which maintain values with RBE > 3 for an extended region. A shift in the RBE maximum can also be observed. The shift is larger for a higher modulation power. As was illustrated in the previous section, the modulation of the particle spectra altered the quality of the mixed radiation field around the Bragg peak area. The modulation enabled primary carbon ions to travel farther than their original maximum range. The displacement of high-LET particles then leads to the shift in the RBE maximum. Consequently, normal lung tissue behind the target is exposed to a higher toxicity than is predicted by the Reference plan. The Optimized plans also exhibit similar broadened RBE distributions as the Degraded plans.

As this is the first work that considered the influence of lung tissue heterogeneities on the RBE-weighted dose, a larger patient study is needed to examine the extent of this biological effect. Ideally a patient-specific modulation power can be used that maps the strength of degradation in each region of the lung. However, as this is currently unattainable, a good alternative would be to use the modulation power as a parameter in a robust optimization algorithm. In addition, the extension of the RBE distribution can also be validated in an in vitro cell experiment. With a more comprehensive investigation, we can assess the clinical relevance of the altered biological effectiveness caused by the spectral modulation.

## 4 | CONCLUSIONS

We presented an adaptation of the TRiP98 treatment planning system that accounted for Bragg peak degradation due to microscopic-scale heterogeneities of lung tissue. The implementation was validated through measurements with carbon ions at the Marburg Ion-Beam Therapy Center. Results from the phantom and patient case studies indicated that the modulation caused underdosage in the target volume and the widening of the distal fall-off. A broader RBE distribution was also observed, imparting a higher toxicity to healthy lung tissues distal to the target. These characteristic features of beam modulation were accurately predicted by the modified dose calculation algorithm. To compensate for the dose perturbations, the implementation was extended to the dose optimization engine. Target

coverage was restored as a result of the optimization. This is the first implementation capable of mitigating for beam modulation in physical and biological inverse treatment planning.

## CONFLICT OF INTEREST

The authors have no conflicts to disclose.

## DATA AVAILABILITY STATEMENT

The data that support the findings of this study are available from the corresponding author on reasonable request.

## REFERENCES

1. Urie M, Goitein M, Holley W, Chen G. Degradation of the Bragg peak due to inhomogeneities. *Phys Med Biol*. 1986;31(1):1-15.
2. Goitein M, Sisterson J. The influence of thick inhomogeneities on charged particle beam. *Radiat Res*. 1978;74:217-230.
3. Pflugfelder D, Wilkens J, Szymanowski H, Oelfke U. Quantifying lateral tissue heterogeneities in hadron therapy. *Med Phys*. 2007;34:1506-1513.
4. España S, Paganetti H. Uncertainties in planned dose due to the limited voxel size of the planning CT when treating lung tumors with proton therapy. *Phys Med Biol*. 2011;56:3843-3856.
5. Titt U, Sell M, Unkelbach J, et al. Degradation of proton depth dose distributions attributable to microstructures in lung-equivalent material. *Med Phys*. 2015;42:6425-6432.
6. Flatten V, Baumann K, Weber U, Engenhart-Cabillic R, Zink K. Quantification of the dependencies of the Bragg peak degradation due to lung tissue in proton therapy on a CT-based lung tumor phantom. *Phys Med Biol*. 2019;64(155005):1-11.
7. Sawakuchi G, Titt U, Mirkovic D, Mohan R. Density heterogeneities and the influence of multiple Coulomb and nuclear scatterings on the Bragg peak distal edge of proton therapy beams. *Phys Med Biol*. 2008;53:4605-4619.
8. Witt M. Modulationseffekte von Kohlenstoffionen bei der Bestrahlung von Lungen. Accessed April 13, 2020. https://www.thm.de/lse/images/user/KZink-105/Abschlussarbeiten/Masterarbeit_Matthias_Witt_2014.pdf.
9. Baumann K, Witt M, Weber U, Engenhart-Cabillic R, Zink K. An efficient method to predict and include Bragg curve degradation due to lung equivalent materials in Monte Carlo codes by applying a density modulation. *Phys Med Biol*. 2017;62:3997-4016.
10. Baumann K, Flatten V, Weber U, et al. Effects of the Bragg peak degradation due to lung tissue in proton therapy of lung cancer patients. *Radiat Oncol*. 2019;14(183):2-15.
11. Ringbæk T, Santiago A, Grzanka L, et al. Calculation of the beam-modulation effect of the lung in carbon ion and proton therapy with deterministic pencil beam algorithms. *Front Phys*. 2020;8(568176):1-13.
12. Winter J, Ellerbrock M, Jäkel O, Greilich S, Bangert M. Analytical modeling of depth-dose degradation in heterogeneous lung tissue for intensity-modulated proton therapy planning. *Phys Imaging Radiat Oncol*. 2020;14:32-38.
13. Tosaki M. Energy-loss straggling caused by the inhomogeneity of target material. *J Appl Phys*. 2006;99(034905):1-8.
14. Schardt D, Elsässer T, Schulz-Ertner D. Heavy-ion tumor therapy: Physical and radiobiological benefits. *Rev Mod Phys*. 2010;82:383-423.
15. Ringbæk T, Simeonov Y, Witt M, et al. Modulation power of porous materials and usage as ripple filter in particle therapy. *Phys Med Biol*. 2017;62:2892-2909.
16. Krämer M, Scholz M, Treatment planning for heavy-ion radiotherapy: calculation and optimization of biologically effective dose. *Phys Med Biol*. 2000;45:3319-3330.
17. Krämer M, Scholz M. Rapid calculation of biological effects in ion radiotherapy. *Phys Med Biol*. 2006;51:1959-1970.
18. Elsässer T, Weyrather WK, Friedrich T, et al. Quantification of the relative biological effectiveness for ion beam radiotherapy: direct experimental comparison of proton and carbon ion beams and a novel approach for treatment planning. *Int J Radiat Oncol Biol Phys*. 2010;78:1177-1183.
19. Press W, Teukolsky S, Vetterling W, Flannery B. *Numerical Recipes in C: The Art of Scientific Computing*. Cambridge University Press; 1992.
20. Krämer M, Jäkel O, Haberer T, Kraft G, Schardt D, Weber U. Treatment planning for heavy-ion radiotherapy: physical beam model and dose optimization. *Phys Med Biol*. 2000;45:3299-3317.
21. Anderle K, Stroom J, Pimentel N, Greco C, Durante M, Graeff C. In silico comparison of photons versus carbon ions in single fraction therapy of lung cancer. *Physica Med*. 2016;32:1118-1123.
22. Chen J, Lu J, Ma N, et al. Early stage non-small cell lung cancer treated with pencil beam scanning particle therapy: retrospective analysis of early results on safety and efficacy. *Radiat Oncol*. 2019;14(16):2-9.
23. Graeff C, Durante M, Bert C. Motion mitigation in intensity modulated particle therapy by internal target volumes covering range changes. *Med Phys*. 2012;39:6004-6013.
24. Chang J, Zhang X, Knopf A, et al. Consensus guidelines for implementing pencil-beam scanning proton therapy for thoracic malignancies on behalf of the PTCOG thoracic and lymphoma subcommittee. *Int J Radiat Oncol Biol Phys*. 2017;99:41-50.
25. Friedrich T, Scholz U, Durante M, Scholz M. RBE of ion beams in hypofractionated radiotherapy (SBRT). *Physica Med*. 2014;30:588-591.
26. van Herk M, Remeijer P, Rasch C, Lebesque J. The probability of correct target dosage: dose-population histograms for deriving treatment margins in radiotherapy. *Int J Radiat Oncol Biol Phys*. 2000;47:1121-1135.
27. van Herk M. Errors and margins in radiotherapy. *Semin Radiat Oncol*. 2004;14:52-64.

**How to cite this article:** Paz AS, Baumann KS, Weber UA, Witt M, Zink K, Durante M, Graeff C. Compensating for beam modulation due to microscopic lung heterogeneities in carbon ion therapy treatment planning. *Med Phys*. 2021;48:8052–8061.
https://doi.org/10.1002/mp.15292